IJC
International Journal of Cancer

Ha-ras and β-catenin oncoproteins orchestrate metabolic programs in mouse liver tumors

Elif B. Unterberger[1], Johannes Eichner[2], Clemens Wrzodek[2], Harri Lempiäinen[3], Raphaëlle Luisier[3], Rémi Terranova[3], Ute Metzger[4], Simon Plummer[5], Thomas Knorpp[4], Albert Braeuning[1], Jonathan Moggs[3], Markus F. Templin[4], Valerie Honndorf[6], Martial Piotto[7], Andreas Zell[2] and Michael Schwarz[1†]

[1] Institute of Experimental and Clinical Pharmacology and Toxicology, Department of Toxicology, Eberhard Karls University of Tübingen, Tübingen 72074, Germany
[2] Center for Bioinformatics Tübingen (ZBIT), Eberhard Karls University of Tübingen, Tübingen 72076, Germany
[3] Discovery and Investigative Safety, Preclinical Safety, Novartis Institutes for Biomedical Research, CH-4057 Basel, Switzerland
[4] Natural and Medical Sciences Institute, University of Tübingen, Reutlingen 72770, Germany
[5] CXR Biosciences, James Lindsay Place, Dundee Technopole, Dundee, Scotland, United Kingdom
[6] Department for Preclinical Imaging and Radiopharmacy, Werner Siemens Imaging Center, Eberhard Karls University, Tübingen 72076, Germany
[7] Bruker Biospin SA, 34, rue de l'Industrie, 67166 Wissembourg Cedex, France

The process of hepatocarcinogenesis in the diethylnitrosamine (DEN) initiation/phenobarbital (PB) promotion mouse model involves the selective clonal outgrowth of cells harboring oncogene mutations in *Ctnnb1*, while spontaneous or DEN-only-induced tumors are often *Ha-ras*- or *B-raf*-mutated. The molecular mechanisms and pathways underlying these different tumor sub-types are not well characterized. Their identification may help identify markers for xenobiotic promoted versus spontaneously occurring liver tumors. Here, we have characterized mouse liver tumors harboring either *Ctnnb1* or *Ha-ras* mutations via integrated molecular profiling at the transcriptional, translational and post-translational levels. In addition, metabolites of the intermediary metabolism were quantified by high resolution ^{1}H magic angle nuclear magnetic resonance. We have identified tumor genotype-specific differences in mRNA and miRNA expression, protein levels, post-translational modifications, and metabolite levels that facilitate the molecular and biochemical stratification of tumor phenotypes. Bioinformatic integration of these data at the pathway level led to novel insights into tumor genotype-specific aberrant cell signaling and in particular to a better understanding of alterations in pathways of the cell intermediary metabolism, which are driven by the constitutive activation of the β-Catenin and Ha-ras oncoproteins in tumors of the two genotypes.

Genotype and phenotype of chemically-induced mouse liver tumors are determined by the treatment regimen.[1] In combination with the initiator N-nitrosodiethylamine (DEN), phenobarbital (PB)-type tumor promoters selectively stimulate the outgrowth of cells harboring activating mutations in the proto-oncogene *Ctnnb1*, which encodes β-Catenin.[2] β-Catenin is a key mediator in the canonical Wnt pathway which activates target gene transcription after forming a complex with members of the TCF/LEF transcription factor family.[3] Without promoter treatment, DEN-initiated mouse liver tumors are mainly *Ha-ras* (∼50%) or *B-raf* (∼20%)-mutated, which leads to constitutive activation of MAPK (mitogen-activated protein

Key words: mouse hepatoma, microarray, tumor metabolism, β-Catenin, Ha-ras

Abbreviations: CAR: constitutive androstane receptor; DEN: N-nitrosodiethylamine; HR-MAS NMR: 1H magic angle nuclear magnetic resonance; InCroMAP: Integrated analysis of Cross-platform MicroArray and Pathway data; LEF-1: lymphoid enhancer factor 1; MAPK: mitogen-activated protein kinase; miRNA: microRNA; Meg3: maternally expressed gene 3; PB: Phenobarbital; PCB: polychlorinated biphenyl; ROS: reactive oxygen species

Additional Supporting Information may be found in the online version of this article.

E.B.U, J.E., C.W., H.L., R.L., R.T., U.M., S.P., T.K., A.B., J.M., M.F.T., V.H., A.Z. and M.S. are members of MARCAR consortium.

Simon Plummer's Current address is: MicroMatrices Associates Ltd, 23 Wellgate Street, Newport-On-Tay, Fife DD6 8HS, Scotland, United Kingdom

Grant sponsor: Innovative Medicine Initiative Joint Undertaking (IMI JU); **Grant number:** 115001 (MARCAR project);
Grant sponsor: NIBR Postdoctoral Fellowship
DOI: 10.1002/ijc.28798
History: Received 31 Oct 2013; Accepted 6 Feb 2014; Online 18 Feb 2014

Correspondence to: Prof. Dr. Michael Schwarz, Institute of Experimental and Clinical Pharmacology and Toxicology, Department of Toxicology, Eberhard Karls University of Tübingen, Wilhelmstr. 56, Tübingen 72074, Germany, Tel.: +[49-7071-29-77398], Fax: +[49-7071-29-2273], E-mail: michael.schwarz@uni-tuebingen.de

What's new?

Changes in tumor cell intermediary metabolism may offer new options in cancer therapy. This study investigated changes in the intermediary metabolism of liver cells caused by aberrant signaling through two different oncoproteins. Mouse liver tumors–either mutated in *Ha-ras* or in *Ctnnb1,* which encodes β-Catenin–were analyzed for changes in global mRNA and microRNA expression, phosphoprotein levels, and metabolite spectra. The study revealed tumor genotype-specific alterations in several important pathways of the cellular intermediary metabolism, increasing knowledge about the complex interplay between oncogenic signaling and the tumor phenotype. This may help advance the diagnostic and development of biomarkers for tumors.

kinase) signaling.[2,4] A wide range of stimuli including mitogenic signals result in Ras-/Raf-mediated activation of downstream kinases which orchestrate target gene expression, thereby regulating proliferation, apoptosis, and intermediary metabolism.[5] Changes in tumor cell intermediary metabolism are of increasing interest and may offer new options in cancer therapy.[6] Such tumor metabolic changes are mostly the result of transcriptional shifts driven by signaling cascades downstream of the activated oncoproteins, but direct metabolic responses to oncoprotein signaling are also well documented.[7] Our previous studies with chemically-induced mouse liver tumors suggest that hepatoma cells adopt very characteristic metabolic programs depending on the oncogene affected by mutation in these cells.[1,8–10] While *Ha-ras*- and *B-raf*-mutated lesions show largely overlapping phenotypes,[8,9] *Ha-ras*- and *Ctnnb1*-mutated tumors differ substantially with regards to their protein and mRNA expression patterns.[1,10] We have now considerably extended our previous studies on mouse liver tumor genotype-phenotype relationships using an integrative molecular and biochemical approach including genome-wide microarray-based transcription (mRNA and microRNA) profiling, pathway-focused reverse phase array analysis of protein expression and post-translational modifications, high resolution ^{1}H magic angle nuclear magnetic resonance (HR-MAS NMR) metabolite profiling and a novel pathway-centric bioinformatic data integration tool.[11] Integrated transcriptomic and biochemical profiling has been successfully used for the molecular classification of various human cancers.[12–14] An advantage of chemically-induced mouse liver tumors, as compared to most human cancers, is the homogeneity in their phenotypic patterns, suggesting that the phenotypic signatures observed directly reflect downstream responses of the activated oncoproteins. Our present data enhance the definition of mouse liver tumor genotype-phenotype relationships and provide new insights into the molecular and biochemical programs triggered by constitutive activation β-Catenin and Ha-ras.

Material and Methods

Study material and animal treatment

Ha-ras-, *B-raf*-, or *Ctnnb1*-mutated tumors and control tissues were generated in previous experiments. In brief, male C3H/HeJ mice received a single *i.p.* injection of DEN (10 or 90 μg/g body weight) at 2 or 6 weeks of age, respectively. After a treatment-free interval of 2 weeks, the C3H/HeJ mice were either kept on a diet containing 0.05% PB or on a PB-free control diet for 28 to 36 weeks before they were sacrificed. Tumors were isolated, flash frozen in liquid nitrogen and stored at −80°C, or prepared for immunohistochemistry as described previously.[15]

Immunohistochemistry and Western blotting

Staining of fixed and embedded liver sections and Western blotting was carried out as previously described.[16]

Mutation analysis

Genomic DNA was isolated from frozen tumor samples. Hotspot site mutations in *Ha-ras* (codon 61) and *B-raf* (codon 637, previously referred to as codon 624) were detected by PCRs and subsequent restriction fragment length polymorphism analyses, as previously described.[17] *Ctnnb1* mutations were identified as described by Aydinlik *et al.*[2]

RNA expression analysis

Affymetrix gene analysis was carried out as previously described.[18] In brief, biotinylated amplified RNA was hybridized to the GeneChip Mouse430_2 arrays. After washing and staining, the arrays were scanned using a solid-state laser scanner (GeneArray Scanner 3000 combined with the GeneChip autoloader, Affymetrix, Santa Clara, CA, USA). The Affymetrix GeneChip Operating Software was used to generate the primary and secondary raw data files.

microRNA expression analysis

Total RNA including miRNA was isolated using the miRNeasy Mini Kit (QIAGEN, Hilden, Germany). RNA integrity was checked with an Agilent 2100 Bioanalyzer using the Agilent RNA 6000 Pico Kit (Agilent Technologies, Santa Clara, CA, USA). Total RNA (25 ng) was end-labeled using the miRNA complete labeling and hybridization kit (Agilent #5190-0456). Agilent unrestricted Mouse miRNA microarrays (8x15K, #G4471A) and Agilent 8x15K gasket slides (#G2534–60015) were used. Arrays were hybridized according to the Agilent miRNA microarray method "miRNA Microarray System with miRNA Complete Labeling and Hyb Kit" (#G4170–90011). Following hybridization and washing, the arrays were scanned on an Agilent Microarray Scanner (#G2505B) according to the manufacturer's protocol. Images were processed using Agilent Feature Extraction Software v9.5.1.

Briefly, miRNA genes that were significantly expressed above background on the individual arrays were identified using Agilent Feature Extraction software. This process involved deletion control and background subtraction and calculation of a *p*-value reflecting the probability that there was no difference in intensity for a given feature to that of a background using a two-sided t-test. The *p*-value calculation was based on an error calculated using an Agilent error model [Agilent Feature Extraction Software (v9.5) #G2566–90012].

Protein expression and post-translational modification analysis

Protein expression profiling on reverse protein arrays was performed as described in Ref. 19 with the following modifications: Tissue lysates were generated by adding an 8-fold excess (vol/wt) of CeLyA Lysis Buffer CLB1 (Zeptosens, Witterswil, Switzerland) containing 1 M NaCl. A microarray layout was chosen that uses two replicates of each sample at a protein concentration of 0.3 mg/ml. Antibodies used for detection of proteins and protein modifications are listed in Supporting Information Table S1. Fluorescence signal was generated using Alexa647- (Invitrogen, Darmstadt, Germany) and Cy5- (Dianova, Hamburg, Germany) labeled secondary antibodies. Microarray images were taken using the ZeptoREADER microarray imager (Zeptosens). Image analysis was performed using the ZeptoVIEW 3.1 software package (Zeptosens).

Metabolite analysis by ^{1}H HR-MAS NMR Spectroscopy

Tissue samples were stored in liquid nitrogen and kept on dry ice during the whole sample preparation process. Approximately 10 mg of tissue and 10 μl of D_2O containing 0.75% (wt/wt) of trimethylsilylproprionate were added to a 33 μl disposable insert made of Kel-F. The D_2O was used to lock the spectrometer and the TSP signal as an indicator of field homogeneity. Spectra were recorded at 277 K at a rotation speed of 5,000 Hz on a 400 MHz Bruker Avance III spectrometer equipped with a SamplePro sample changer and a HR-MAS probe (Bruker Biospin, Wissembourg, France). 1D-^{1}H CPMG (Carr-Purcell-Meiboom-Gill) spectra with water presaturation were recorded with the following parameters: 128 scans, 20 ppm sweep width, 4 sec relaxation delay, 4 sec acquisition time and 75 msec spin-spin relaxation time. 2D NMR experiments (^{1}H-^{13}C HSQC, ns = 128, ^{1}H-^{1}H TOCSY, ns = 64, mixing time = 60 msec) were obtained to confirm the identification of the metabolites. Bruker software packages were used to process and analyze the spectra (Topspin 3.2). 2D spectra were analyzed using the Sparky software (http://www.cgl.ucsf.edu/home/sparky). Additionally, metabolites were identified based on literature data.[20–22] Quantification of the metabolites was assessed using a standard insert of sucrose containing 20 μl of a 9.9 mM solution of sucrose in D_2O corresponding to a total of 198 nmoles of sucrose.

Bioinformatic data processing

mRNA. The Affymetrix CEL files containing the raw probe intensities were normalized using the Robust Multichip Average method. The quality of the experiments was assessed using diverse plots and statistics implemented in the package arrayQualityMetrics for R/Bioconductor.[23] Based on extensive quality controls, we concluded that all arrays had sufficient quality. A moderated t-statistic was chosen to detect differentially expressed genes (implementation from limma package for R/Bioconductor[24]). The Benjamini-Hochberg method was applied to correct for testing multiple genes.

microRNA. Background correction and pooling of probe signal levels corresponding to the individual miRNAs was performed using the Agilent Feature Extraction (AFE) image analysis algorithm from the AgiMicroRna package for R/Bioconductor.[25] Probe sets which were flagged as not expressed by the AFE software in all samples were excluded from further analysis. Afterwards, the mean fold changes were computed for each replicate group and *p*-values were computed using a moderated t-test with FDR (false discovery rate) correction. Experimentally verified mRNA targets of miRNAs were extracted and merged from the publicly available databases miRecords v3, miRTarBase v2.4 and TarBase v5.0c.

Protein expression/post-translational modifications

Annotation with UniProt IDs, log-transformation and median-centering was applied to the data in order to ease the interpretability and to obtain a symmetrical scale of the protein and protein-modification levels. Measurements for which the background noise (signal of secondary antibody) was higher than the combined foreground and background signal (signal of primary and secondary antibody) were treated as missing values (<1%) and imputed using the k-Nearest-Neighbor (kNN) algorithm. For the detection of differential protein expression, we employed the same procedure as described for mRNA data except that we lowered the cutoff values to a fold change of $|\log\text{-ratio}| > 0.585$.

Software

The visualizations in Figure 3 and Supporting Information Figure S1 were created using BioDraw Ultra 12.0 (PerkinElmer, Cambridge, MA, USA).

Results

Mutation analysis

Twenty-seven chemically-induced mouse liver tumors[26–28] were screened for *Ha-ras*, *B-raf*, and *Ctnnb1* mutations. The tumors used in the present study—which had been induced originally in our laboratory for a different purpose—were "new" in that they had not been investigated before for the presence of mutations or for phenotypic changes. The results (Supporting Information Table S2) confirmed our previous data showing that the mutation frequencies of the proto-oncogenes strongly depend on the treatment regimen.[2] Due to the known similarities between *Ha-ras*- and *B-raf*-mutated mouse hepatomas,[8,9] only tumors mutated in either *Ha-ras* or *Ctnnb1* and corresponding normal tissue samples were

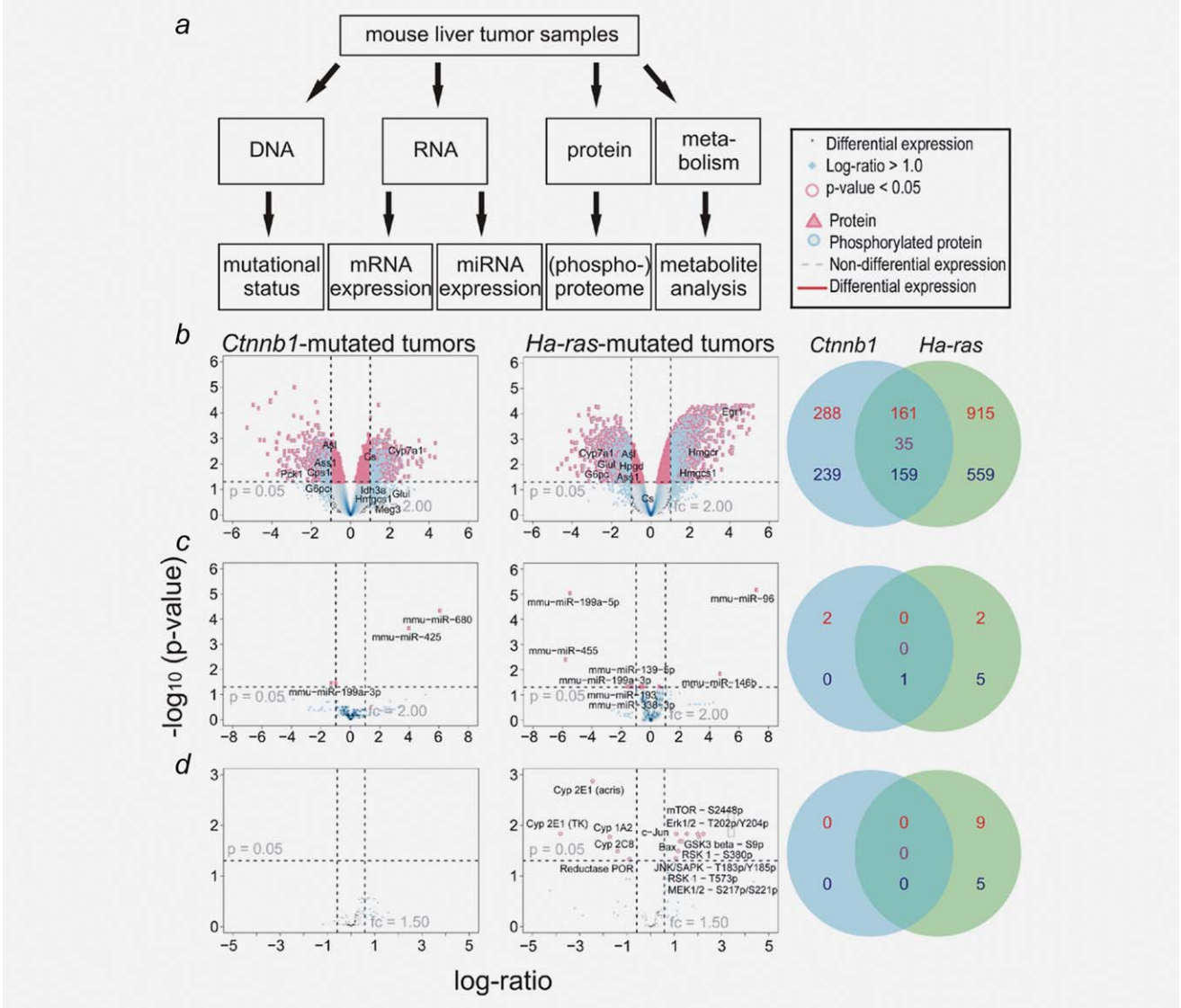

Figure 1. (*a*) Workflow of the analysis of *Ha-ras*- and *Ctnnb1*-mutated mouse liver tumors. (*b-d*) Results of global statistical analysis of (*b*) mRNA, (*c*) miRNA, and (*d*) protein expression and phosphorylation in *Ha-ras*- and *Ctnnb1*-mutated mouse liver tumors. Red numbers in the Venn diagrams stand for up-regulation, blue numbers for down-regulation and purple numbers for inverse regulation. Significance requirements: |log-ratio| >1.0 (>0.585 for protein data), *p*-value <0.05.

subjected to the further analyses outlined in Figure 1*a*. To exclude an occult contamination of normal liver tissue with tumor tissue to the greatest possible extent, we checked for mRNA expression of the tumor marker Afp (α-fetoprotein) in the control samples. Three samples with increased Afp levels were excluded from further analysis. In total, for the further analyses, we included 7 *Ctnnb1*-mutated tumors along with three control tissues from DEN/PB-treated mice and three *Ha-ras*-mutated tumors along with three control tissues from DEN only-treated mice.

Tumor genotype-specific changes in mRNA, miRNA, protein and phosphoprotein expression

Tumors were characterized with respect to changes in their transcriptome, their miRNA profile, and their protein expression and phosphorylation patterns. A global picture illustrating the molecular changes at the different levels is depicted in Figure 1. To this end, the log 2 fold-changes of tumor vs. normal tissue, referred to as "log-ratios" in the figures and manuscript, were computed. As criteria of significance, absolute |log-ratios| >1.0 (protein: >0.585) and FDR-corrected *p*-values <0.05 were chosen. For datasets see: http://www.ncbi.nlm.nih.gov/geo/query/acc.cgi?acc=GSE51358.

mRNA expression. *Ha-ras*- and *Ctnnb1*-mutated hepatomas showed clear differences in their gene expression patterns (Fig. 1*b*). 288 probe sets were exclusively up-regulated in *Ctnnb1*-mutated compared to 915 in *Ha-ras*-mutated tumors. Another 161 were concomitantly increased in both types of lesions. About half of the down-regulated probe sets in

Table 1. List of miRNAs with significantly differential expression in *Ctnnb1*- and/or *Ha-ras*-mutated tumors (|log-ratio| >1.0, *p*-value <0.05)

		Ctnnb1-mutated		*Ha-ras*-mutated		
miRNA name	Ensembl gene ID	Log-ratio	*p*-value	Log-ratio	*p*-value	Experimentally validated targets[1]
mmu-miR-680	ENSMUSG00000076253	6.11	<0.01			
mmu-miR-425	ENSMUSG00000065579	4.01	<0.01			
mmu-miR-96	ENSMUSG00000065586			7.21	<0.01	Odf2, Celsr2, Myrip, Aqp5, Ryk
mmu-miR-199a-5p	ENSMUSG00000070126			−5.45	<0.01	Sirt1, Hif1a
mmu-miR-455	ENSMUSG00000070102			−5.74	<0.01	
mmu-miR-146b	ENSMUSG00000070127			4.75	0.01	
mmu-miR-338-3p	ENSMUSG00000065600			−1.54	0.05	
mmu-miR-139-5p	ENSMUSG00000065446			−1.21	0.05	Foxo1
mmu-miR-193	ENSMUSG00000065395			−1.41	0.05	
mmu-miR-199a-3p	ENSMUSG00000070126	−1.25	0.04	−1.23	0.05	Smad1

[1]Experimentally validated target mRNAs were annotated according to the miRecords v3, miRTarBase 2.4 and TarBase V5.0c databases.

Ctnnb1-mutated tumors was also decreased in the *Ha-ras*-mutated ones (159 of 398). All in all, the *Ha-ras*-mutated tumors contained 718 down-regulated probe sets. 35 probe sets showed anti-correlated expression, *i.e.*, were either up-regulated in *Ha-ras*- and down-regulated in *Ctnnb1*-mutated tumors, or *vice versa* (for complete gene lists see Supporting Information Tables S3 and S4). Many of the changes at the mRNA level were also observed previously by our group.[1,9]

miRNA expression. In total, only 10 miRNAs met the criteria of significance (Fig. 1*c* and Table 1), suggesting limited perturbations of this class of non-coding RNA. In addition to the experimentally validated target mRNAs listed in Table 1, predicted mRNA targets were identified according to the databases ElMMo,[29] DIANA microT[30] and TargetScan.[31] However, only one predicted target was significantly changed in the present study, namely *Tgfb2* (encoding transforming growth factor β2), which is targeted by *miR-199a-5p* and was up-regulated in *Ha-ras*-mutated tumors. Consistently, *miR-199a-5p* was strongly decreased in these lesions.

Protein and phosphoprotein levels. Antibodies (130 in total) for the reverse phase protein microarray analysis were chosen with a focus on xenobiotic-metabolizing enzymes and protein kinases with a role in signaling. Several kinases were changed in their level and hyperphosphorylated in *Ha-ras*-mutated tumors as compared to normal liver, while none of the proteins met the criteria of significance in *Ctnnb1*-mutated tumors (Fig. 1*d*). Additional information is given in Supporting Information Table S5. The predicted changes in signaling pathways deduced from the changes in RNA and protein/phosphoprotein patterns are summarized in Supporting Information Figure S1A/B.

Integrated analysis of tumor genotype-specific changes in metabolic pathways

Activation of β-Catenin or Ha-ras was associated with specific changes in mRNAs encoding enzymes of the intermediary metabolism (for a list of enzymes see Supporting Information Table S6). Changes were analyzed on a global basis using the cross-platform data analysis tool InCroMAP,[11] a novel software tool allowing powerful high-level cross-platform microarray dataset analysis and visualization. Pathway enrichment procedures were applied to the mRNA expression datasets and significantly altered metabolic pathways were color-labeled according to their *p*-value in the KEGG global metabolic pathway map,[32] as shown in Figure 2. Gross inspection of the two KEGG pathway maps revealed striking differences between the metabolic networks of the two tumor genotypes. In total, 36 metabolic KEGG pathways were significantly altered in *Ha-ras*-mutated tumors, as compared to 21 pathways in their *Ctnnb1*-mutated counterparts (indicated by light to dark blue color; a scalable version of the underlying KEGG pathway graph is shown in Supporting Information Figure S2; for a detailed list of pathways and genes involved see Supporting Information Table S7). We stratified the metabolic pathways into 5 classes (numbers of pathways in square brackets): amino acid metabolism [13], carbohydrate and energy metabolism [8], lipid metabolism [12], xenobiotic and drug metabolism [3] and other pathways [3]. For validation purposes, we also included mRNA profiling from our previous studies on *Ctnnb1*-, *Ha-ras*-, or *B-raf*-mutated tumors.[1,9,33] Moreover, since zonal expression of metabolic enzymes in the liver is affected by Wnt/β-Catenin- and Ha-ras-dependent signaling,[16,34,35] we also compared the tumor results with our previous data on global gene expression in periportal and perivenous hepatocytes.[34] The complete dataset is summarized in Supporting Information Table S7. Selected highlights are discussed below and summarized in Figure 3 and in Supporting Information Figures S3 and S4.

Carbohydrate and energy metabolism. *Ha-ras*- and *Ctnnb1*-mutated tumors both showed a reduction in mRNA expression of glucose-6-phosphatase (*G6pc*), which catalyzes the

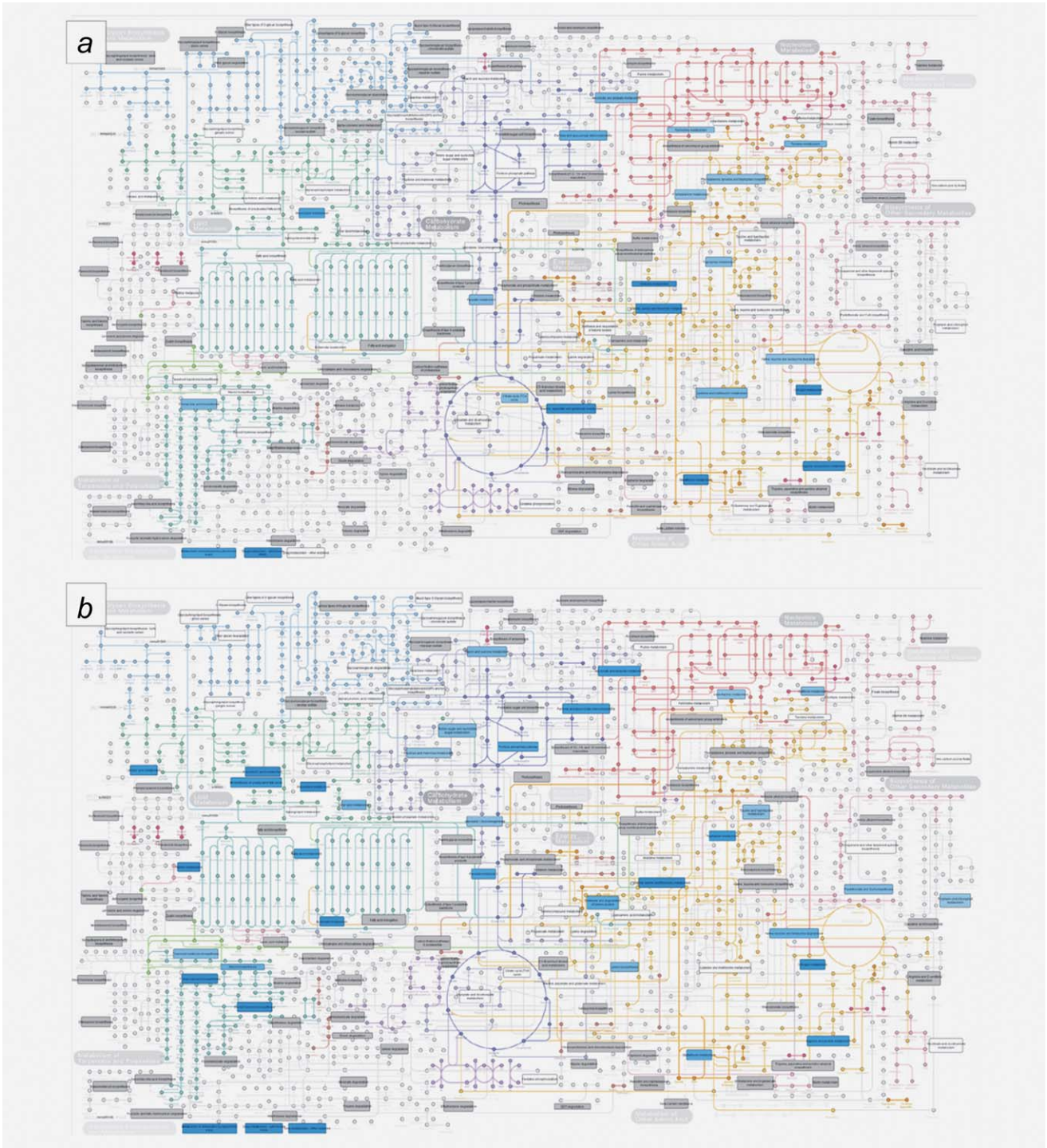

Figure 2. Visualization of global mRNA enrichments in metabolic pathways in (*a*) Ctnnb1- and (*b*) Ha-*ras*-mutated tumors. Rectangular boxes refer to referenced pathways, enrichment *p*-values are depicted by the following color code: grey is used for pathways that are not contained in the enrichment. White indicates non-significant differential expression (enrichment *p*-value >0.05), blue indicates significant *p*-values (<0.05) and a more saturated color is used for lower *p*-values.

last step of gluconeogenesis. Similarly, mRNA for *Pck1*, which encodes the rate-controlling gluconeogenic enzyme phosphoenol pyruvate carboxykinase was decreased in both tumor types. Expression of citrate synthase (*Cs*) and a subunit of isocitrate dehydrogenase (*Idh3a*), the rate-limiting enzyme of the TCA cycle, were up-regulated in *Ctnnb1*– but down-regulated in *Ha-ras*-mutated tumors; the fold changes of both enzymes in *Ha-ras*-mutated tumors were below our cutoff levels of 1.0, despite *p*-values <0.05. miR-23a, which targets the transcript of *G6pc*,[36] was increased in

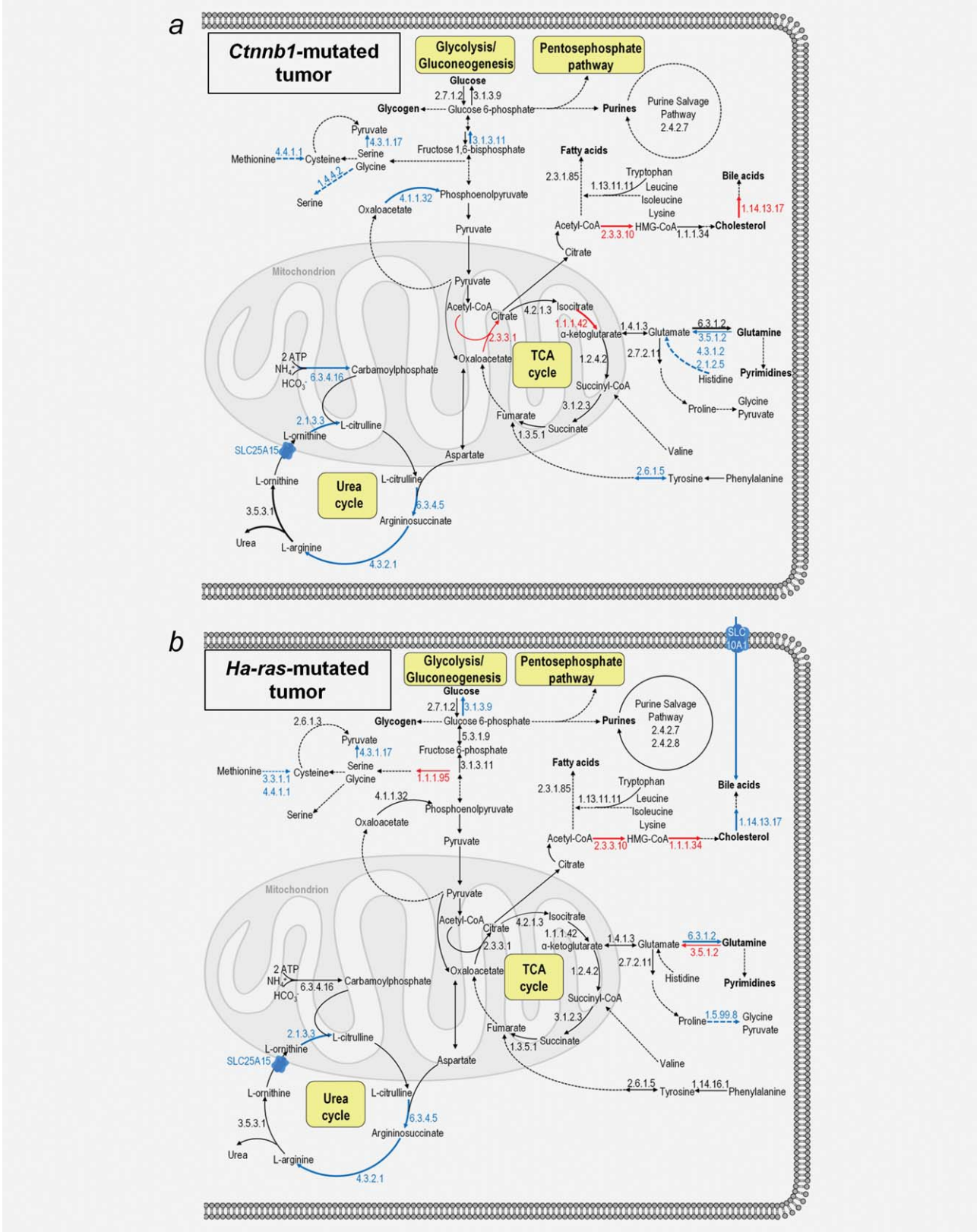

Figure 3. Changes in mRNA expression in central metabolic pathways in (*a*) *Ctnnb1*-mutated and (*b*) *Ha-ras*-mutated tumors. Reactions catalyzed by individual enzymes are indicated by arrows and enzyme codes, dotted arrows stand for a series of enzymatic reactions. Red arrows indicate significantly up-regulated, blue arrows significantly down-regulated mRNAs (p-value <0.05, $|\text{log-ratio}| > 1.0$). For corresponding enzyme names and gene symbols see Supporting Information Table S6.

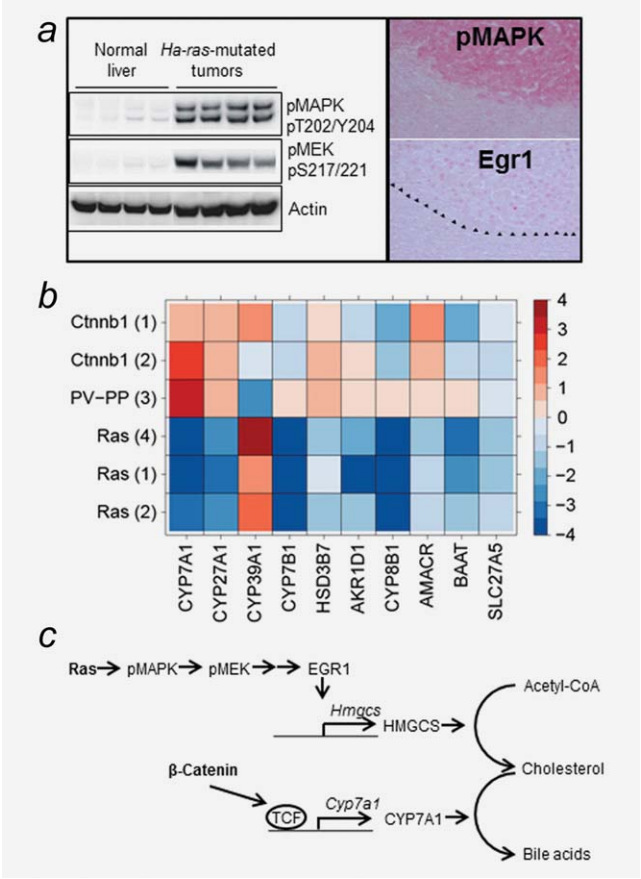

Figure 4. Cholesterol and bile acid biosynthesis as case study for integrative data analysis. (*a*) Activated phospho-forms of MAPK (pMAPK) and MEK (pMEK) protein are up-regulated in *Ha-ras*-mutated tumors as detected by Western analysis (left part) and immunostaining (right part). Immunostaining for the transcription factor EGR1 demonstrates its nuclear localization in the pMAPK-positive *Ha-ras* mutated tumor. (*b*) Heatmap indicating the changes in mRNA expression relative to normal liver in *Ctnnb1* (Ctnnb1)- and *Ha-ras* (Ras)-mutated tumors and in perivenous as compared to periportal (PV-PP) hepatocytes. The data are taken from this and previous studies from our group: (1) reference 1; (2) present paper; (3) reference 33; (4) reference 9. (*c*) Summary of tumor genotype-specific differences in regulation of cholesterol and primary bile acid biosynthesis predicted by changes in mRNA levels and signaling proteins.

Ha-ras-mutated tumors by a factor of 1.08 and a *p*-value slightly higher than the required cutoff (0.063). Loss of glucose-6-phosphatase activity is frequently observed in liver tumors, and might result in increased levels of glucose-6-phosphate which can be utilized in the pentose phosphate pathway. Two genes of this pathway encoding X-linked glucose-6-phosphate dehydrogenase and phosphogluconate dehydrogenase were significantly upregulated in *Ha-ras*-mutated tumors (Fig. 3).

Lipid metabolism. Changes in the expression of genes encoding enzymes of lipid metabolism were a hallmark of *Ha-ras*-mutated tumors, with 12 KEGG pathways affected (Fig. 2). Genes involved in cholesterol and bile acid metabolism were changed in both tumors. HMG-CoA synthase 1 (*Hmgcs1*) was up-regulated in both tumor types, whereas HMG-CoA reductase (*Hmgcr*) was only up-regulated in *Ha-ras*-mutated tumors (Fig. 3). *Hmgcs1* is transactivated by activated MAPK via the transcription factor EGR1 (early growth response 1),[37] which was accordingly up-regulated in *Ha-ras*-mutated tumors (Supporting Information Table S4A). *Ctnnb1*-mutated tumors showed increased expression of cholesterol 7α-hydroxylase (*Cyp7a1*), which catalyzes the rate-limiting step of bile acid biosynthesis from cholesterol (Fig. 3), while Cyp7a1 together with all but one other mRNAs encoding enzymes of bile acid biosynthesis were down-regulated in *Ha-ras*-mutated tumors (for an overview see Fig. 4). Transcription of several other enzymes involved in steroid biosynthesis, however, was up-regulated in *Ha-ras*-mutated tumors, including 7-dehydrocholesterol reductase (*Dhcr7*), squalene epoxidase (*Sqle*) and lanosterol synthase (*Lss*), whereas most enzymes of steroid hormone biosynthesis were down-regulated.

In *Ha-ras*-mutated tumors, the majority of genes involved in arachidonic acid degradation were significantly down-regulated. Similarly, several genes involved in linoleic acid degradation were decreased. A number of desaturases (*Fads1*, *Fads2*, *Scd2*) assigned to the metabolism of unsaturated fatty acids were significantly up-regulated in *Ha-ras*-mutated tumors. With regards to fatty acid metabolism in general, no consistent direction of transcriptional change was observed in the two tumor types.

The mRNA encoding *Gpam*, which catalyzes the initial and committing step of glycerolipid synthesis, was significantly up-regulated in *Ha-ras*-mutated tumors. Consistently, monoacylglycerol lipase (*Mgll*) and hepatic lipase (*Lipc*), which hydrolyze glycerides, were transcriptionally down-regulated in these tumors.

β-Carotene 15,15'-monooxygenase (*Bcmo1*), essential for activation of retinol and other vitamin A forms, was transcriptionally up-regulated in *Ha-ras*-mutated tumors, as was retinol dehydrogenase 5 (*Rdh5*), which mediates the final step of 11-cis retinaldehyde biosynthesis. By contrast, several Cyps and alcohol dehydrogenase 4 (*Adh4*), which metabolize retinol, were down-regulated in *Ha-ras*-mutated tumors.

Amino acid and nitrogen metabolism. In agreement with earlier observations,[1] many genes involved in amino acid degradation were down-regulated in *Ctnnb1*- and (this paper) *Ha-ras*-mutated tumors. Several of these genes and genes encoding enzymes of energy metabolism are direct β-Catenin/TCF targets[38]; they are listed in Supporting Information Table S8. We also confirmed the complete down-regulation of urea cycle enzymes in *Ctnnb1*-mutated tumors seen in our previous study.[1]

Xenobiotic metabolism. A synopsis of the observed changes is summarized in Supporting Information Table S7. In very general terms, mRNAs for phase I and phase II metabolism of drugs and xenobiotics were mostly down-regulated in *Ha-ras*-mutated tumors and often up-regulated in their

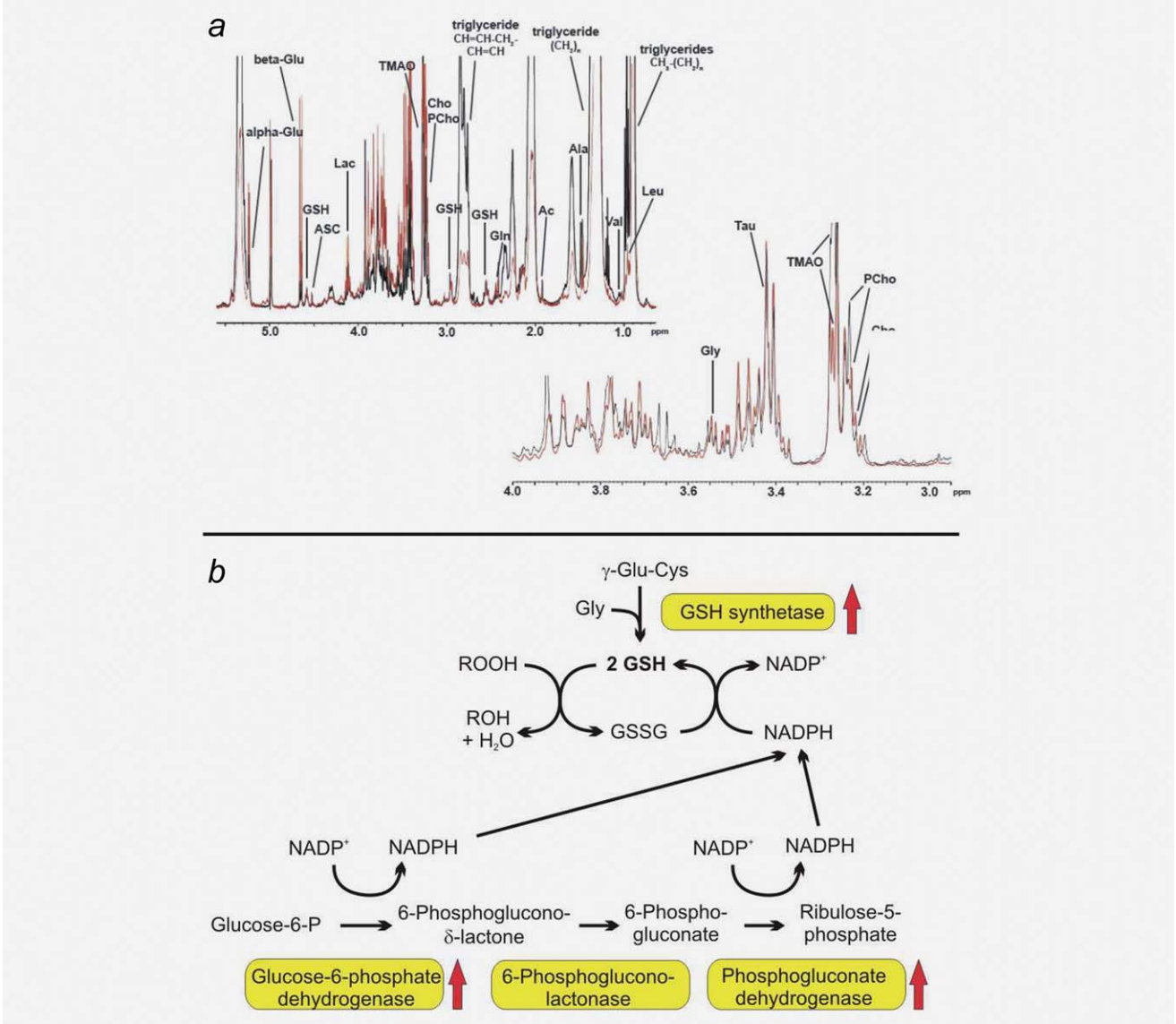

Figure 5. (*a*) Tumor metabolite spectra as analyzed by HR-MAS NMR; the red spectrum is representative for a *Ha-ras*-mutated tumor; the black spectrum represents the respective normal liver. (*b*) Changes in mRNAs encoding enzymes of glutathione metabolism in *Ha-ras*-mutated tumors (indicated by red / blue arrows). HR-MAS NMR demonstrated increase in glutathione in tumors of this genotype.

Ctnnb1-mutated counterparts, with some exceptions. This is in accordance with previous studies from our group.[8,10]

HR-MAS NMR analysis of tumor metabolite spectra

We were able to clearly identify 16 different metabolites of the intermediary metabolism, of which 11 could be quantified unequivocally (Supporting Information Table S9). Representative 1D and 2D spectra are shown in Figure 5*a* and Supporting Information Figure S5. Most of the metabolites were unchanged in the tumors. Changes in comparison to the respective normal tissues were only seen in *Ha-ras*-mutated tumors, where the levels of valine, glutathione and lactate were increased, while β-D-glucose was decreased.

Discussion

We have identified mouse liver tumor genotype-specific differences in mRNA, miRNA and protein/phosphoprotein expression that facilitate the molecular and biochemical stratification of tumor phenotypes. A similar question was adressed in a previous study from our group.[1] The results of the present study are based on an entirely new set of tumors and - different from the previous study - tumor-surrounding normal liver from PB-treated mice was included as a control, which allowed us to discriminate effects produced by PB from those which are tumor-specific. Moreover, we not only investigated changes in global mRNA expression but we also determined, in the very same tumors, changes in miRNA, protein, phosphoprotein and metabolite levels, enabling us to

generate a very comprehensive overview on tumor genotype-specific changes.

We first analyzed changes at the mRNA and protein level in signaling pathways and found very characteristic changes in tumors of the two genotypes (Supporting Information Fig. S1). The present study, however, concentrates on changes in tumor intermediary metabolism. Our data reveal that activation of the *Ha-ras* or *Ctnnb1* proto-oncogenes results in distinct tumor genotype-specific metabolic programs spanning carbohydrate, amino acid, lipid, and xenobiotic metabolism.

Both *Ctnnb1*- and *Ha-ras*-mutated tumors showed decrease in *Pck1* encoding phosphenolpyruvate carboxykinase 1, which predicts a down-regulation of gluconeogenesis. *G6pc* mRNA and the activity of glucose-6-phosphatase (determined by enzyme histochemistry; Supporting Information Fig. S6), were also decreased. Integration of mRNA and miRNA data revealed a potential mechanism for G6pc down-regulation in *Ha-ras*-mutated tumors, whereby miR-23 targets the *G6pc* transcript and thus inhibits its translation.[36] The fact that miR-23a was up-regulated only in *Ha-ras*- but not in *Ctnnb1*-mutated tumors while G6pc is reduced in both tumor types implies that alternative regulatory mechanisms for G6pc down-regulation must exist. Decrease in glucose-6-phosphatase activity is of advantage for tumor cells since it will trap glucose as energy source.

Glucose-6-phosphate can fuel glycolysis but may also be utilized through the pentose-phosphate pathway. The latter is predicted to be up-regulated in *Ha-ras*-, but not in *Ctnnb1*-mutated tumors, based on increases in the mRNAs encoding glucose-6-phosphate dehydrogenase and phosphogluconate dehydrogenase (Supporting Information Fig. S7). An increase in the flux through the pentose-phosphate pathway will produce NADPH required for the detoxification of reactive oxygen species (ROS) which are often elevated in tumor cells.[39] Glutathione synthetase was significantly increased in *Ha-ras*-mutated tumors in this and two previous studies[1,9]; it is required for the synthesis of glutathione which is a key molecule in ROS detoxification. Glutathione levels were in fact increased in *Ha-ras*- but not in *Ctnnb1*-mutated tumors (Supporting Information Table S9). For an overview on changes in glutathione metabolism in *Ha-ras*-mutated tumors see Figure 5*b*.

According to the Warburg effect, rather than metabolizing pyruvate aerobically in the TCA cycle, tumors produce energy via glycolysis and subsequent lactate fermentation, converting pyruvate into lactate via lactate dehydrogenase, which is transcriptionally up-regulated in MYC-induced mouse hepatomas.[40] Interestingly, neither *Ctnnb1*- nor *Ha-ras*-mutated tumors in our study showed increased levels of *Ldh* mRNA. Lactate levels were slightly enhanced in *Ha-ras*- but not in *Ctnnb1*-mutated tumors (Supporting Information Table S9). Furthermore, we observed slight transcriptional up-regulation of the TCA cycle enzymes isocitrate dehydrogenase (*Idh3a*) and citrate synthase (*Cs*) in *Ctnnb1*-mutated tumors. Together, these results point to aerobic glucose metabolism in the *Ctnnb1*-mutated lesions, contrary to Warburg's theory. This is supported by Yuneva *et al.*[40] who did not detect increased lactate levels in MET-induced mouse liver tumors which contain activated β-Catenin.

Genes encoding enzymes of nitrogen and amino acid metabolism were altered in both tumor types, which are in accordance with previous results on mRNA expression[1] and recently conducted ChIP-sequencing data from tissues with either activated or inhibited β-Catenin.[38] Interestingly, the down-regulation of genes related to amino acid degradation, urea cycle, and gluconeogenesis in *Ctnnb1*-mutated tumors (Table 2) correlates with their periportal localization in normal liver (see also Table 2 and Ref. 41). Thus, our results are consistent with the observation that *Ctnnb1*-mutated tumor tissue shows the perivenous phenotype and periportal gene expression is most likely suppressed in these tumors, whereas the periportal phenotype is induced in *Ha-ras*-mutated tumors.[16,33] This statement is not restricted to nitrogen and amino acid metabolism: The side-to-side listing of the gene expression results in the *Ctnnb1*- and *Ha-ras*-mutated liver tumors along with the perivenous versus periportal expression values in the Supporting Information Table S7 allows a direct comparison of changes within individual metabolic pathways. The color codes (blue = significantly down-regulated; red = significantly up-regulated) allow a simple comparison. If significant changes occur for individual genes, they go, in almost 100% of cases, into the same direction for *Ctnnb1*-mutated tumors and perivenous versus periportal hepatocytes.

In normal liver, *Pck1* and *G6pc* are expressed in periportal hepatocytes and are transcriptionally activated by HNF4α,[42] which was unchanged in both our mRNA and protein datasets. However, it has recently been shown that β-Catenin, which is constitutively active in *Ctnnb1*-mutated tumors, acts as a direct negative regulator of both *Pck1* and *G6pc* in a complex with TCF4,[38] consistent with our data.

The number of aberrantly expressed genes encoding enzymes involved in lipid metabolism was higher in *Ha-ras*- as compared to *Ctnnb1*-mutated tumors, and the majority of genes were down-regulated in the former tumors. An exception was *Hmgcs*, encoding HMG-CoA synthase 1 (*Hmgcs1*), the rate-limiting enzyme of the mevalonate pathway and HMG-CoA-reductase (*Hmgcr*), which are key to cholesterol biosynthesis. We were not able to detect the two enzymes at the protein level with commercially available antibodies by immunohistochemical staining or Western Blot. However, our recent 2D-PAGE and MALDI-TOF-TOF analysis proves that Hmgcs is up-regulated in *Ha-ras*-mutated tumors.[8] Dysregulation of the mevalonate pathway by increased Hmgcs activity promotes cell transformation.[43] Proliferating tumor cells require cholesterol for membrane synthesis and increased levels of the steroid may be advantageous for them.[9] Both *Hmgcs* and *Hmgcr* are known targets of the transcription factor EGR1,[37] which was up-regulated at the mRNA and protein levels in the *Ha-ras*-mutated tumors in our study. This is consistent with the previous finding that *Egr1* expression is activated by MAPK signaling via a serum

response element in the promoter region of the gene.[44,45] Accordingly, we found increased levels of activated MAPK and increased *Egr1* expression in the *Ha-ras*-mutated tumors. Cholesterol accumulation in *Ha-ras*-mutated tumors has previously been shown by our group.[9] These results suggest an induction of cholesterol biosynthesis by MAPK signaling via EGR1 in tumors harboring *Ha-ras*-mutations (Fig. 4).

Cholesterol levels in *Ha-ras*-mutated tumors are not only increased by elevated synthesis but likely also by reduced efflux to bile acid synthesis. Remarkably, all but one (Cyp39a1) of the genes encoding enzymes involved in the metabolism of cholesterol to bile acids were strongly down-regulated in *Ha-ras*-mutated tumors, including Cyp7a1, catalyzing the first step in the metabolic cascade (Fig. 4*b*). Therefore, the Ha-ras oncoprotein exerts a potent negative-regulatory effect on the entire metabolic cascade by a yet unknown mechanism.

In sharp contrast to *Ha-ras*-mutated tumors, *Cyp7a1* was up-regulated in *Ctnnb1*-mutated tumors, suggesting positive control of the gene by the Wnt/β-catenin pathway. In normal liver, *Cyp7a1* mRNA expression is higher in perivenous than in periportal hepatocytes (Fig. 5 and Supporting Information Table S7), and perivenous gene expression is regulated by β-Catenin.[16,34,35] An *in silico* analysis identified binding sites for the transcription factors TCF and HNF4 in the *Cyp7a1* promoter (not shown), which suggests that *Cyp7a1* is under genetic regulation by β-Catenin. These data therefore predict increased synthesis of primary bile acids in *Ctnnb1*-mutated tumors while their levels may be decreased in their *Ha-ras*-mutated counterparts.

In conclusion, our analyses revealed tumor genotype-specific alterations in several important pathways of the cellular intermediary metabolism, increasing our knowledge about the complex interplay between oncogenic signaling and the resulting tumor phenotype. Knowledge about metabolic reprogramming in tumor cells is of potential interest for diagnostic purposes and the development of tumor biomarkers but may also lead to previously unexpected cancer treatment strategies.[6]

Acknowledgements

The authors thank all members of the MARCAR consortium. The excellent technical support by Elke Zabinsky is greatly acknowledged. They thank Michael Römer for help with GEO submission of data. H.L. is the recipient of a NIBR Postdoctoral Fellowship.

Author contributions

All authors designed and conducted the experiment and reviewed the manuscript; JE, CW, EBU, MS and AB analyzed and interpreted data; EBU, MS and AB wrote the paper.

References

1. Stahl S, Ittrich C, Marx-Stoelting P, et al. Genotype-phenotype relationships in hepatocellular tumors from mice and man. *Hepatology* 2005;42:353–61.
2. Aydinlik H, Nguyen TD, Moennikes O, et al. Selective pressure during tumor promotion by phenobarbital leads to clonal outgrowth of β-catenin-mutated mouse liver tumors. *Oncogene* 2001;20:7812–16.
3. Behrens J, Kries JPv, Kühl M, et al. Functional interaction of β-catenin with the transcription factor LEF-1. *Nature* 1996;382:638–41.
4. Jaworski M, Buchmann A, Bauer P, et al. *B-raf* and *Ha-ras* mutations in chemically induced mouse liver tumors. *Oncogene* 2005;24:1290–5.
5. Dhillon AS, Hagan S, Rath O, et al. MAP kinase signalling pathways in cancer. *Oncogene* 2007;26:3279–90.
6. Schulze A, Harris AL. How cancer metabolism is tuned for proliferation and vulnerable to disruption. *Nature* 2012;491:364–73.
7. Ward PS, Thompson CB. Metabolic reprogramming: a cancer hallmark even warburg did not anticipate. *Cancer Cell* 2012;21:297–308.
8. Rignall B, Ittrich C, Krause E, et al. Comparative transcriptome and proteome analysis of Ha-ras and B-raf mutated mouse liver tumors. *J Proteome Res* 2009;8:3987–94.
9. Jaworski M, Ittrich C, Hailfinger S, et al. Global gene expression in Ha-ras and B-raf mutated mouse liver tumors. *Int J Cancer* 2007;121:1382–5.
10. Strathmann J, Paal K, Ittrich C, et al. Proteome analysis of chemically induced mouse liver tumors with different genotype. *Proteomics* 2007;7:3318–31.
11. Wrzodek C, Eichner J, Zell A. Pathway-based visualization of cross-platform microarray datasets. *Bioinformatics* 2012;28:3021–6.
12. Kristensen VN, Vaske CJ, Ursini-Siegel J, et al. Integrated molecular profiles of invasive breast tumors and ductal carcinoma in situ (DCIS) reveal differential vascular and interleukin signaling. *Proc Natl Acad Sci USA* 2012;109:2802–7.
13. Martín-Subero JI, Kreuz M, Bibikova M, et al. New insights into the biology and origin of mature aggressive B-cell lymphomas by combined epigenomic, genomic, and transcriptional profiling. *Blood* 2009;113:2488–97.
14. Shen L, Toyota M, Kondo Y, et al. Integrated genetic and epigenetic analysis identifies three different subclasses of colon cancer. *Proc Natl Acad Sci* 2007;104:18654–9.
15. Loeppen S, Koehle C, Buchmann A, et al. A β-catenin-dependent pathway regulates expression of cytochrome P450 isoforms in mouse liver tumors. *Carcinogenesis* 2005;26:239–48.
16. Hailfinger S, Jaworski M, Braeuning A, et al. Zonal gene expression in murine liver: lessons from tumors. *Hepatology* 2006;43:407–14.
17. Buchmann A, Karcier Z, Schmid B, et al. Differential selection for *B-raf* and *Ha-ras* mutated liver tumors in mice with high and low susceptibility to hepatocarcinogenesis. *Mutat Res* 2008;638:66–74.
18. Lempiainen H, Muller A, Brasa S, et al. Phenobarbital mediates an epigenetic switch at the constitutive androstane receptor (CAR) target gene Cyp2b10 in the liver of B6C3F1 mice. *PLoS One* 2011;6:e18216.
19. Braeuning A, Heubach Y, Knorpp T, et al. Gender-specific interplay of signaling through beta-catenin and CAR in the regulation of xenobiotic-induced hepatocyte proliferation. *Toxicol Sci* 2011;123:113–22.
20. Benahmed MA, Santelmo N, Elbayed K, et al. The assessment of the quality of the graft in an animal model for lung transplantation using the metabolomics 1H high-resolution magic angle spinning NMR spectroscopy. *Magn Reson Med* 2012;68:1026–38.
21. Castejon D, Villa P, Calvo MM, et al. 1H-HRMAS NMR study of smoked Atlantic salmon (Salmo salar). *Magn Reson Chem* 2010;48:693–703.
22. Rooney OM, Troke J, Nicholson JK, et al. High-resolution diffusion and relaxation-edited magic angle spinning 1H NMR spectroscopy of intact liver tissue. *Magn Reson Med* 2003;50:925–30.
23. Kauffmann A, Gentleman R, Huber W. arrayQualityMetrics—a bioconductor package for quality assessment of microarray data. *Bioinformatics* 2009;25:415–16.
24. Smyth GK. Linear models and empirical bayes methods for assessing differential expression in microarray experiments. *Stat Appl Genet Mol Biol* 2004;3:Article3.
25. Lopez-Romero P. Pre-processing and differential expression analysis of Agilent microRNA arrays using the AgiMicroRna Bioconductor library. *BMC Genomics* 2011;12:64.
26. Rignall B, Braeuning A, Buchmann A, et al. Tumor formation in liver of conditional beta-catenin-deficient mice exposed to a diethylnitrosamine/phenobarbital tumor promotion regimen. *Carcinogenesis* 2010;32:52–7.
27. Jaworski M, Hailfinger S, Buchmann A, et al. Human p53 knock-in (hupki) mice do not differ in liver tumor response from their counterparts with murine p53. *Carcinogenesis* 2005;26:1829–34.

28. Marx-Stoelting P, Mahr J, Knorpp T, et al. Tumor promotion in liver of mice with a conditional Cx26 knockout. *Toxicol Sci* 2008;103: 260–7.
29. Gaidatzis D, van Nimwegen E, Hausser J, et al. Inference of miRNA targets using evolutionary conservation and pathway analysis. *BMC Bioinformatics* 2007;8:69.
30. Maragkakis M, Vergoulis T, Alexiou P, et al. DIANA-microT Web server upgrade supports Fly and Worm miRNA target prediction and bibliographic miRNA to disease association. *Nucleic Acids Res* 2011;39:W145–W148.
31. Friedman RC, Farh KK, Burge CB, et al. Most mammalian mRNAs are conserved targets of microRNAs. *Genome Res* 2009;19:92–105.
32. Kanehisa M, Goto S, Sato Y, et al. KEGG for integration and interpretation of large-scale molecular data sets. *Nucleic Acids Res* 2012;40: D109–D114.
33. Braeuning A, Ittrich C, Kohle C, et al. Zonal gene expression in mouse liver resembles expression patterns of Ha-ras and beta-catenin mutated hepatomas. *Drug Metab Dispos* 2007;35:503–7.
34. Braeuning A, Ittrich C, Kohle C, et al. Differential gene expression in periportal and perivenous mouse hepatocytes. *FEBS J* 2006;273:5051–61.
35. Benhamouche S, Decaens T, Godard C, et al. Apc tumor suppressor gene is the "zonation-keeper" of mouse liver. *Dev Cell* 2006;10:759–70.
36. Wang B, Hsu SH, Frankel W, et al. Stat3-mediated activation of microRNA-23a suppresses gluconeogenesis in hepatocellular carcinoma by down-regulating Glucose-6-phosphatase and peroxisome proliferator-activated receptor gamma, coactivator 1 alpha. *Hepatology* 2012;56:186–97.
37. Gokey NG, Lopez-Anido C, Gillian-Daniel AL, et al. Early growth response 1 (Egr1) regulates cholesterol biosynthetic gene expression. *J Biol Chem* 2011;286:29501–10.
38. Gougelet A, Torre C, Veber P, et al. T-cell factor 4 and beta-catenin chromatin occupansies pattern zonal liver metabolism. *Hepatology* 2013. Doi: 10.1002/hep.26924.
39. Anastasiou D, Poulogiannis G, Asara JM, et al. Inhibition of pyruvate kinase M2 by reactive oxygen species contributes to cellular antioxidant responses. *Science* 2011;334:1278–83.
40. Yuneva MO, Fan TW, Allen TD, et al. The metabolic profile of tumors depends on both the responsible genetic lesion and tissue type. *Cell Metab* 2012;15:157–70.
41. Gebhardt R. Metabolic zonation of the liver: regulation and implications for liver function. *Pharmacol Ther* 1992;53:275–354.
42. Hall RK, Sladek FM, Granner DK. The orphan receptors COUP-TF and HNF-4 serve as accessory factors required for induction of phosphoenolpyruvate carboxykinase gene transcription by glucocorticoids. *Proc Natl Acad Sci USA* 1995;92: 412–16.
43. Clendening JW, Pandyra A, Boutros PC, et al. Dysregulation of the mevalonate pathway promotes transformation. *Proc Natl Acad Sci USA* 2010;107:15051–6.
44. Gregg J, Fraizer G. Transcriptional regulation of EGR1 by EGF and the ERK signaling pathway in prostate cancer cells. *Genes Cancer* 2012;2:900–9.
45. Qureshi SA, Cao XM, Sukhatme VP, et al. v-Src activates mitogen-responsive transcription factor Egr-1 via serum response elements. *J Biol Chem* 1991;266:10802–6.